Controlling the Orientation of Hexapole-Selected Hydroxyl (OH) Radicals

Toby D. Hain[†] **and Thomas J. Curtiss***[,‡]

Department of Chemistry, University of Utah, Salt Lake City, Utah 84112

Received: May 27, 1998; In Final Form: July 27, 1998

Recently, Hain, Toby D.; Weibel, Michael A.; Backstrand, Kyle M.; and Curtiss, Thomas J. *J. Phys. Chem. A* **1997**, *101*, 7674 reported the production of intense, rotationally state-selected, supersonic beams of hydroxyl radicals via electric hexapole focusing. Here, a detailed description of the lab frame orientation of selected radicals is provided. The distribution of orientations can be systematically varied with the electric field strength in a post-hexapole scattering region. This control of orientation results from the field-dependent mixing of the different parity states comprising the OH Λ-doublets. Calculated fluorescence yields show polarization-dependent LIF measurements probe the alignment terms of the orientation distribution, and field-dependent measurements probe the parity state composition.

1. Introduction

Interest in stereodynamics, the study of correlations among *vectorial* properties in chemical dynamics, has been escalating in recent years, primarily due to advances in both theoretical and experimental methods.[1−8] Vectorial properties consist of velocity distributions in the lab and center-of-mass reference frames as well as distributions of rotational and electronic angular momenta among reactants and products. Understanding the stereodynamic details of reactive collisions provides the most intimate glimpse possible of the potential energy surface (or surfaces) mediating the forces among atoms that lead to chemical changes, particularly near the critical transition-state region. Stereodynamic measurements, therefore, provide very useful data for making comparisons with developing scattering theories and ab initio calculations of potential energy surfaces.[9−11]

Experimental efforts generally focus on two objectives: the precollision preparation of the vectorial properties of reagents[3,7,12−15] and probing the vectorial properties of post-collision products.[16,17] In spirit with the former, Hain, et al.[18,19] and Schreel, et al.[20,21] have recently prepared high-intensity molecular beams of rotationally state-selected hydroxyl radicals using electrostatic hexapole focusing techniques.[7,22−24] In this article we provide detailed descriptions of the highly anisotropic distributions of molecular orientations (or, equivalently, rotational angular momenta) characterizing these beams and of the exquisite experimental control we have over these distributions. We also outline results expected from polarization-dependent laser induced fluorescence experiments designed to validate our calculated orientational distributions. Much of the formalism used in this article has been published previously.[19,25]

The orientational control we now have over hydroxyl radicals creates new opportunities to probe the stereodynamics of reactive collisions in the gas phase (e.g., OH + H−X → H_2O + X; X = H,[26] CH_3,[27] NH_2,[28] Cl,[29] etc.) and with surfaces.[30,31] The OH + H_2 reaction is particularly important and has, in recent years, become the bellwether in quantum scattering studies of four-atom reactions.[32]

2. Theory of Orientation

In this section we describe the rich and subtle behavior of the orientation of the molecular axis in the laboratory-frame of hydroxyl radicals in rotational states selected by an electrostatic hexapole. We shall direct our attention specifically toward the dependence of the orientation on the electric field strength in the region following the hexapole state-selector. We will see that the complexity introduced to the rotational behavior by the effects of Λ-doubling also provides the means to systematically tune the distribution of orientations experimentally.

The electron configuration for the OH radical is $(1s\sigma)^2$ $(2s\sigma)^2$ $(2p\sigma)^2$ $(2p\pi)^3$, with an inverted $^2\Pi_{3/2}$ ground state. In a Hund's case (a) coupling scheme, the projection of the operators **L**, the electronic orbital angular momentum, and **S**, the electronic spin angular momentum, onto the molecular axis commute with the Hamiltonian leading to the good quantum numbers Λ (±1) and Σ ±$^1/_2$ respectively. The numbers in parentheses indicate possible values for a $^2\Pi$ state. The projection of the total angular momentum **J** also commutes leading to the quantum number Ω (= Λ + Σ = ± $^3/_2$, ± $^1/_2$). Our basis functions for describing hexapole selected wave functions are $|n\,^2\Pi_\Omega\, v\, J\, M\rangle$ which may be separated into electronic orbital, electronic spin, rotational, and vibrational components: $|n\Lambda\rangle\,|S\Sigma\rangle\,|J\Omega\, M\rangle\,|v\rangle$. The rotational wave functions $|J\ \Omega\ M\rangle$ are given by the corresponding symmetric top wave functions:[33]

$$|J\Omega M\rangle \equiv \left[\frac{2J+1}{4\pi}\right]^{1/2} D^{J*}_{M\,\Omega}(\varphi,\theta,0) \qquad (1)$$

and contain all the information regarding the orientation of the molecular axes with respect to laboratory-frame coordinates. Figure 1 shows a vector model representation of the $|J\ \Omega\ M\rangle$ rotational basis wave functions corresponding to the lowest $J = {}^3/_2$ rotational energy level. Classically, the molecular axis $\hat{z}$ precesses around the total angular momentum vector **J** that in

[†] E-mail: tdhain@chemistry.chem.utah.edu.
[‡] E-mail: curtiss@chemistry.chem.utah.edu.

10.1021/jp9823906 CCC: $15.00
Published on Web 11/04/1998

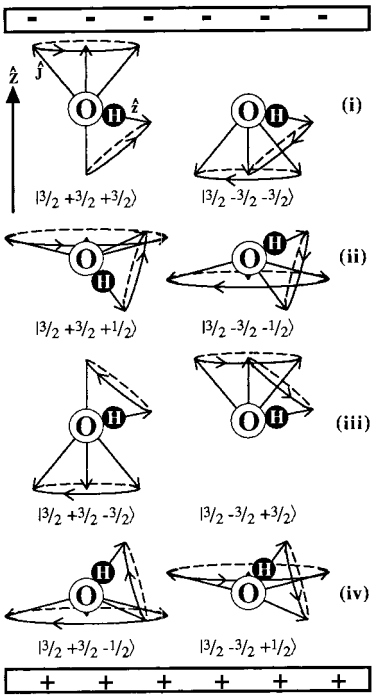

Figure 1. Vector models showing the precessional motion possible for various rotational states of OH for $J = |\Omega| = {}^3/_2$. The models are grouped into four pairs: pairs (i) and (ii) are successfully transmitted by a hexapole state selector while pairs (iii) and (iv) are rejected by the state selector (see text for discussion).

turn precesses around the laboratory-frame quantization axis $\hat{Z}$.[34] It is evident in Figure 1 that, within each of the following pairs:

$$|{}^3/_2 + {}^3/_2 + {}^3/_2\rangle \qquad |{}^3/_2 - {}^3/_2 - {}^3/_2\rangle \qquad \text{(i)}$$

$$|{}^3/_2 + {}^3/_2 + {}^1/_2\rangle \qquad |{}^3/_2 - {}^3/_2 - {}^1/_2\rangle \qquad \text{(ii)}$$

$$|{}^3/_2 + {}^3/_2 - {}^3/_2\rangle \qquad |{}^3/_2 - {}^3/_2 + {}^3/_2\rangle \qquad \text{(iii)}$$

$$|{}^3/_2 + {}^3/_2 - {}^1/_2\rangle \qquad |{}^3/_2 - {}^3/_2 + {}^1/_2\rangle \qquad \text{(iv)}$$

the wave functions differ only with regard to the direction of their precessional motion, and the distributions of the orientation of the molecular $\hat{z}$ axis with respect to the quantization axis $\hat{Z}$ (i.e., $\hat{z}\cdot\hat{Z}$) is identical for each pair. Consequently, we often designate these pairs together, e.g., as $|{}^3/_2 \pm {}^3/_2 \pm {}^3/_2\rangle$[35] for the first pair, or simply as $|{}^3/_2\ {}^3/_2\ {}^3/_2\rangle$.

As we will demonstrate shortly, these eight wave functions are eigenfunctions for a Hund's case (a) molecule in the limit of high electric field strength. The high field limit is the electric field strength required to approximately reach the highest degree of orientation of the molecular axis with respect to the laboratory frame. Furthermore, an electric hexapole can be used to selectively focus a molecular beam of molecules in the first two pairs of states [(i) and (ii)] while rejecting the last two pairs [(iii) and (iv)]. Most $^2\Pi$ diatomic radicals are intermediate between Hund's case (a) and (b) due to spin−orbit mixing, becoming more (b)-like as J increases. For OH, the low J states being considered in this discussion are greater than 93% Hund's case (a).[19] Spin−orbit mixing is easily incorporated by constructing wave functions from linear combinations of the two spin−orbit state wave functions corresponding to $|\Omega| = {}^3/_2$ and ${}^1/_2$.[19,33] In all calculations described in this article, spin−orbit mixing has been included, but for simplicity we retain the *labels* corresponding to the dominant Hund's case (a) spin−orbit state. Because the unpaired electron in OH is localized in an oxygen atom p orbital, the Fermi contact and pseudodipolar electron−nuclear spin terms are small in OH.[36] Therefore, J is a good quantum number,[37] and hyperfine effects on the focusing behavior, which can often be significant,[38] can be ignored. Furthermore, for the electric field strengths used in our calculations, negligible mixing of J-levels occur. We have calculated the off-diagonal elements of the Stark matrix (J-mixing terms) and find that they contribute less than a factor of 10^{-6} to the overall Stark energies. The rotational energy difference between the $J = {}^3/_2$ and $J = {}^5/_2$ levels in the $\Omega = {}^3/_2$ spin−orbit manifold is 88 cm^{-1}, much too far apart to be coupled by the applied electric field strengths used in this study. In the brute force orientation method used by several groups,[3,14,15,39] polar molecules with large dipole moments and small rotational constants ($\mu_{OH} = 1.67$ D and $B_{OH} = 18.5$ cm^{-1} vs $\mu_{KCl} = 10.24$ D and $B_{KCl} = 0.114$ cm^{-1}) are placed in field strengths on the order of 10^4 kV cm^{-1} compared to our highest field strengths of 100 kV cm^{-1}. Extensive rotational state mixing occurs due to closely spaced rotational levels in a large magnitude field producing the net orientation.

In the absence of an electric field, the parity operator commutes with the Hamiltonian. We construct wave functions of definite parity by taking symmetric and antisymmetric combinations of the $|J\ \Omega\ M\rangle$ wave functions corresponding to the models in Figure 1:[19,33]

$$\Psi_1^0 = \frac{1}{\sqrt{2}}(|J\Omega M\rangle + |J - \Omega M\rangle)$$

$$\Psi_2^0 = \frac{1}{\sqrt{2}}(|J\Omega M\rangle - |J - \Omega M\rangle) \qquad (2)$$

As the OH radical rotates, electronic motion does not follow the nuclear motion exactly causing an energy splitting between the states labeled by the preceding wave functions; this splitting is termed Λ-doubling.[40]

In the presence of an external electric field, parity is no longer well defined, and the field will mix rotational states in the two parity subgroups yielding coupled wave functions:[41]

$$\Psi_1 = a(\epsilon)\Psi_1^0 + b(\epsilon)\Psi_2^0$$

$$\Psi_2 = -b(\epsilon)\Psi_1^0 + a(\epsilon)\Psi_2^0 \qquad (3)$$

where the mixing coefficients depend on the magnitude of the electric field

$$a(\epsilon) = \left[\frac{\sqrt{\nu_\lambda^2 + (2\epsilon\mu\langle\cos\theta\rangle)^2} + \nu_\lambda}{2\sqrt{\nu_\lambda^2 + (2\epsilon\mu\langle\cos\theta\rangle)^2}}\right]^{1/2}$$

$$b(\epsilon) = \left[\frac{\sqrt{\nu_\lambda^2 + (2\epsilon\mu\langle\cos\theta\rangle)^2} - \nu_\lambda}{2\sqrt{\nu_\lambda^2 + (2\epsilon\mu\langle\cos\theta\rangle)^2}}\right]^{1/2} \qquad (4)$$

with

$$\langle\cos\theta\rangle = \frac{\Omega M}{J(J+1)} \qquad (5)$$

and $\nu_\Lambda \equiv$ lambda-doublet splitting frequency, $\mu \equiv$ permanent electric dipole moment, and $\epsilon \equiv$ electric field strength. Note that, in the above expression for $\langle\cos\theta\rangle$, Ω is the weighted

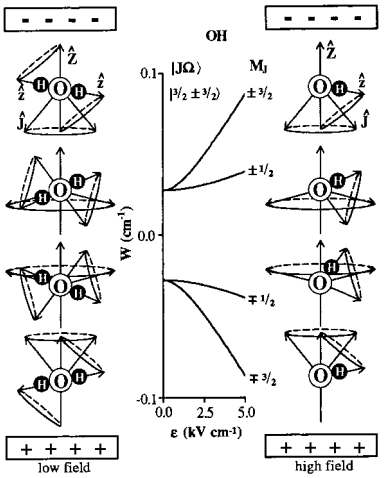

Figure 2. Stark energy plot for the $|^3/_2\ ^3/_2\ M\rangle$ rotational states of the hydroxyl radical with accompanying classical precessional vector models. Models on the left depict the precessional motion in the low-field limit, models on the right in the high-field limit.

sum of contributions from each spin−orbit state. Of the two wave functions appearing in 3, Ψ_1 is selectively focused by the hexapole. It is instructive to note that in the limit as $\epsilon \rightarrow$ *high field*, $a(\epsilon) = b(\epsilon) = 1/\sqrt{2}$, indicating that the basis functions depicted in Figure 1 are indeed eigenfunctions in the high field limit. In the limit as $\epsilon \rightarrow 0$, $a(\epsilon) = 1$, and $b(\epsilon) = 0$, indicating that the eigenfunctions in the limit of low field are composed of a 50% mixture of basis functions. It is important to keep in mind that in a field-free region ($\epsilon = 0$) the quantization axis becomes arbitrary, effectively randomizing the quantum states among all possible M values within a Λ-doublet branch for a given J and Ω. This results in an isotropic distribution of orientations. Previously, the energies of these coupled wave functions (eq 3) were calculated as a function of field strength for OH,[19,25] results we have reproduced here for OH in Figure 2. The energetics are essential for determining the force applied to a molecule by the inhomogeneous hexapole field and simulating experimentally measured focusing spectra. This was the central theme of Hain's article.[19] Here our primary interest is in quantifying the orientational behavior of these coupled wave functions as a function of field strength.

Located on the left- and right-hand sides of Figure 2 are vector models of the classical precessional motion of the hydroxyl radical in an electric field in the limit of low and high field strength, respectively.[34] The $\hat{J}$ vector represents a unit vector in the direction of the total angular momentum vector. For the four models presented, $\hat{J}$ makes different angles with respect to $\hat{Z}$ for the classical models of the $|M| = {}^3/_2$ states and the $|M| = {}^1/_2$ states. This corresponds to the degree of orientation. For the states with $|M| = {}^3/_2$, the motion of the H atom is more tightly constrained around $\hat{Z}$ than for the $|M| = {}^1/_2$ states. Both classically and quantum mechanically at $|\hat{z}\cdot\hat{Z}| = |\cos\theta| = 1$, the $|M| = {}^1/_2$ states have nodes in contrast to the $|M| = {}^3/_2$ states. As might be expected, in the *high-field* limit the oxygen atom end of radicals in rotational states whose energies increase with field strength spend more time near the negative electrode than do the more electropositive hydrogen atom end. The opposite is true for the states whose energies decrease with increasing field strength. Those states with a positive Stark effect, i.e., increasing energies, are repelled by regions of high field near the electrodes of the hexapole and are selectively focused back toward the hexapole symmetry axis.

The orientation for a given rotational state can be quantified by calculating the orientational probability distribution functions, the probability of finding the molecular axis pointing in the solid angle element $d\cos\theta$. The classical recipe has been given elsewhere,[34] and quantum calculations have been published for the orientational probability distribution functions $P(\cos\theta)$ of several rotational states of OH in the limit of high field.[19,25] However, since the wave functions are electric field dependent, the orientational probability distribution functions are electric field dependent as well, $P(\cos\theta, \epsilon)$. The $P(\cos\theta, \epsilon)$ may be written in terms of a Legendre series expansion or may be cast in terms of Wigner rotation functions $d(\theta)$ (the χ and ϕ components have been integrated out):

$$P(\cos\theta,\epsilon) = [a(\epsilon) + b(\epsilon)]^2\left(\frac{2J+1}{4}\right)d^J_{M\,\Omega}(\theta)(-1)^{M-\Omega}d^J_{-M-\Omega}(\theta) + [a(\epsilon) - b(\epsilon)]^2\left(\frac{2J+1}{4}\right)d^J_{M-\Omega}(\theta)(-1)^{M+\Omega}d^J_{-M\,\Omega}(\theta)$$

$$= \left(\frac{2J+1}{4}\right)\sum_{n=0}^{2J}(2n+1)\begin{pmatrix} J & J & n \\ M & -M & 0\end{pmatrix}P_n(\cos\theta)\times \left\{[a(\epsilon) + b(\epsilon)]^2(-1)^{M-\Omega}\begin{pmatrix} J & J & n \\ \Omega & -\Omega & 0\end{pmatrix} + [a(\epsilon) - b(\epsilon)]^2(-1)^{M+\Omega}\begin{pmatrix} J & J & n \\ -\Omega & \Omega & 0\end{pmatrix}\right\} \quad (6)$$

The odd terms in the Legendre expansion, i.e., $n = 1$, 3, etc. are commonly referred to as orientational terms while the even n-components are alignment terms. Equation 6 may be written as

$$P(\cos\theta) = {}^1/_2(2J+1)\sum_{n=0}^{2J}C_n(\epsilon)P_n(\cos\theta) \quad (7)$$

where the limiting case expansion coefficients are

$$C_n(\epsilon \rightarrow 0) = {}^1/_2(2n+1)\begin{pmatrix} J & J & n \\ M & -M & 0\end{pmatrix}\left\{(-1)^{M-\Omega}\begin{pmatrix} J & J & n \\ \Omega & -\Omega & 0\end{pmatrix} + (-1)^{M+\Omega}\begin{pmatrix} J & J & n \\ -\Omega & \Omega & 0\end{pmatrix}\right\}$$

$$C_n(\epsilon \rightarrow \textit{high field}) = (2n+1)(-1)^{M-\Omega}\begin{pmatrix} J & J & n \\ \Omega & -\Omega & 0\end{pmatrix}\begin{pmatrix} J & J & n \\ M & -M & 0\end{pmatrix} \quad (8)$$

Table 1 shows individual expansion terms in the low- and high-field limits for selectable rotational states including spin−orbit mixing. Figure 3 shows the $P(\cos\theta, \epsilon)$ as surface contour plots for several rotational states of OH. The $\cos\theta$ axis has three limiting behaviors indicated with tick marks: for $\cos\theta = +1$, μ is parallel to ϵ (molecular axis antiparallel); for $\cos\theta = 0$, μ is perpendicular to ϵ (molecular axis also perpendicular); and for $\cos\theta = -1$, μ is antiparallel to ϵ (molecular axis parallel). The maximum electric field strengths shown are 90% of the high-field limit. Figure 3 demonstrates the remarkable experimental control we have over the orientations of hexapole-selected beams. One can tune the hexapole voltage into resonance with a specific pair of high field rotational states, e.g., the $|^3/_2 \pm {}^3/_2 \pm {}^3/_2\rangle$, states, and, by varying the electric field strength of the orienting field following the hexapole, one may continuously vary the orientational probability distribution

TABLE 1: Electric Field Dependent Orientational Probability Distribution Coefficients Including Spin−Orbit Mixing

$\|J\Omega M\rangle$	ϵ	C_0	C_1	C_2	C_3	C_4	C_5
$^3/_2 \pm {}^3/_2 \pm {}^3/_2$	0	0.25	0	0.235	0		
$^3/_2 \pm {}^3/_2 \pm {}^1/_2$	0	0.25	0	−0.235	0		
$^5/_2 \pm {}^3/_2 \pm {}^5/_2$	0	0.167	0	−0.072	0	−0.095	0
$^5/_2 \pm {}^3/_2 \pm {}^3/_2$	0	0.167	0	0.014	0	0.284	0
$^5/_2 \pm {}^3/_2 \pm {}^1/_2$	0	0.167	0	0.058	0	−0.189	0
$^1/_2 \pm {}^1/_2 \pm {}^1/_2$	0	0.5	0				
$^3/_2 \pm {}^3/_2 \pm {}^3/_2$	hf[a]	0.25	0.441	0.235	0.044		
$^3/_2 \pm {}^3/_2 \pm {}^1/_2$	hf	0.25	0.147	−0.235	−0.132		
$^5/_2 \pm {}^3/_2 \pm {}^5/_2$	hf	0.167	0.204	−0.072	−0.189	−0.095	−0.016
$^5/_2 \pm {}^3/_2 \pm {}^3/_2$	hf	0.167	0.123	0.014	0.264	0.284	0.078
$^5/_2 \pm {}^3/_2 \pm {}^1/_2$	hf	0.167	0.041	0.058	0.151	−0.189	−0.157
$^1/_2 \pm {}^1/_2 \pm {}^1/_2$	hf	0.5	0.5				

[a] hf is the high-field limit.

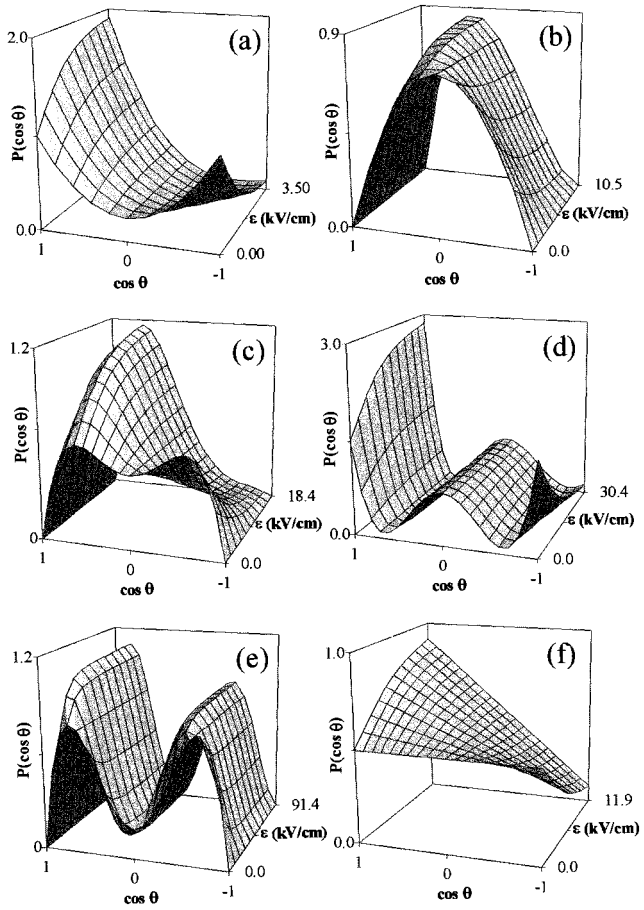

Figure 3. Electric field dependent orientational probability distribution functions for the: (a) $|^3/_2 \pm {}^3/_2 \pm {}^3/_2\rangle$, (b) $|^3/_2 \pm {}^3/_2 \pm {}^1/_2\rangle$, (c) $|^5/_2 \pm {}^3/_2 \pm {}^5/_2\rangle$, (d) $|^5/_2 \pm {}^3/_2 \pm {}^3/_2\rangle$, (e) $|^5/_2 \pm {}^3/_2 \pm {}^1/_2\rangle$, and (f) $|^1/_2 \pm {}^1/_2 \pm {}^1/_2\rangle$ rotational states for the hydroxyl radical are shown as contour plots with varying electric field strengths.

function in a systematic way. For example, at $\epsilon \approx 0$ kV cm^{-1}, the low-field limit, all distributions are symmetric about $\cos\theta = 0$, and the axis distribution is aligned with the orientation moments C_n (odd n) zero (see Table 1). Increasing the orienting field voltage to the high-field limit, one obtains an oriented molecular axis ensemble.

3. LIF: A Test of the Orientational Distribution

In the previous section we developed the formalism necessary to calculate the electric field dependent orientational probability distribution functions for hexapole state-selected molecular beams of OH. One would like to validate these predictions experimentally. In this section we discuss how this might be accomplished by measuring the polarization dependence of OH laser induced fluorescence (LIF). LIF detection of OH radicals is well established.[42] Greene and Zare[43] have provided the theoretical machinery to analyze LIF spectra to determine the population and alignment of a molecular beam ensemble. Their study involved the use of linearly polarized radiation pumping a well-known absorption line with resolved or unresolved emission and emphasized the analysis of an initial cylindrically symmetric ensemble of molecules. This method may be employed to measure the alignment distribution in rotational states selected by the hexapole and probed by the laser. The post-hexapole field varies the parity state composition of the selected OH beam. Probing a single parity level, i.e., parity of sharp angular momentum, with LIF enables us to measure these compositional changes.

The LIF intensity is given by[43]

$$I \propto \sum_{\alpha',\alpha'',k_d,k_a,k} S(J',\alpha';J'',\alpha'')\mathbf{E}(k_d,k_a,k,0;\Omega)A_0^{(k)} \times \omega(k_d,k_a,k;J_i'',J',J_f'') \quad (9)$$

where α' and α'' are all quantum numbers needed to fully describe the upper ($'$) and lower ($''$) states, respectively; S is the line strength factor, $\mathbf{E}$ is the polarization tensor, A is the alignment parameter, and ω is the angular momentum recoupling factor between initial ($J_i''\alpha''$), excited ($J'\alpha'$) and final states ($J_f''\alpha''$) of the LIF process. Multipole moments of the detected, absorbed, and overall fluorescence process, are represented by k_d, k_a, and k, respectively. The line strength is given by[25]

$$S(|A^2\textstyle\sum^+ J'(\Omega' = 1/2)M'p^-\rangle; |X^2\Pi_{3/2}J''(\Omega'' = {}^3/_2)M''p^-\rangle) \propto c^2(\epsilon)(2J''+1)(2J'+1)\left[b_{J''}^2\begin{pmatrix} J'' & 1 & J' \\ -{}^3/_2 & 1 & {}^1/_2\end{pmatrix} \pm a_{J''}^2\begin{pmatrix} J'' & 1 & J' \\ -{}^1/_2 & 1 & -{}^1/_2\end{pmatrix}\right]^2 \begin{pmatrix} J'' & 1 & J' \\ -M'' & -\Delta M & M'\end{pmatrix}^2 f(\theta_0) \quad (10)$$

where

$$f(\theta_0) = \begin{cases} {}^1/_2[1+\cos^2(\theta_0)] & \text{for} \quad \Delta M = \pm 1 \\ \sin^2(\theta_0) & \text{for} \quad \Delta M = 0 \end{cases} \quad (11)$$

and $c^2(\epsilon)$ is either $a^2(\epsilon)$ or $b^2(\epsilon)$ [see eq 4 and discussion below] depending on which Λ-doublet is being probed, p'' represents the parity of the rotational level, the coefficients $a_{J''}^2$ and $b_{J''}^2$ effectively take into account spin−orbit coupling in the $^2\Pi_\Omega$ rotational states, and the θ_0 is the angle between the laboratory-frame orienting electric field vector and the laser polarization vector. Greene and Zare consider an LIF scheme where averaging is done over the initial state's magnetic sublevels, M_i''; in our treatment we do not average over M_i'' since we have selected a particular pair of $|J\Omega M\rangle$ substates. Recall $|J\Omega M\rangle$ represents $|J|\Omega||M|\rangle$ and $|J-|\Omega|-|M|\rangle$. Inherent in their treatment of LIF is the geometrical and dynamical processes responsible for the polarization and direction of absorbed and detected photons. The alignment of the initial state of sharp angular momentum, prepared via the hexapole and oriented in the post-hexapole field, is described by the alignment terms $A_0^{(k)}$. Emitted photons arising from a polarized absorption event will have an anisotropic spatial distribution attributed to the dipole nature of absorption and emission.[43] The direction of absorbed

and emitted photons (along with the experimental configuration described below: perpendicular arrangement of quantization axis, pump laser, and detector) is contained in the polarization tensor **E** and angular momenta recoupling factors ω in eq 9.

For the system being considered, the spatial distribution of molecular axes has been described in the previous section. We assume the molecules are in a homogeneous electric field as before with the quantization axis defined by the local electric field vector, the laboratory frame *Z* axis, and the molecular axis defines the molecule-fixed *z* axis. The laboratory frame *X* axis is the propagation direction of a linearly polarized laser beam, and the laboratory frame *Y* axis is defined by the direction of the photomultiplier detector which only collects a fraction of the emitted photons (those propagating in the detector direction along *Y*). These coordinates satisfy Greene and Zare's mutually orthogonal geometry requirements for probe and detector positions. The polarization of the excitation laser is scanned through 90°, and the detected fluorescence is nondispersed without intervening polarization optics.

In our scheme, the laser pumps a single $|J\Omega M\rangle$,-selected state rotational line of given parity. For OH at zero field, the upper Λ-doublet is of f symmetry and is probed via Q ($\Delta N = 0$) lines, and the lower component is of e symmetry which is probed by P ($\Delta N = -1$) and R ($\Delta N = +1$) lines.[44] For the component selected by the hexapole, the state increases from being pure f symmetry at zero field (Q lines) to mixed e/f symmetry at high field (see eq 3); therefore, only a fraction of the molecules in a hexapole-selected rotational state may be excited. Greater attention is called to the electric field dependent e/f symmetry effect in subsequent paragraphs. Considering only perpendicular $Q_1(N'')$ ($\Delta N = 0$) transitions in the $A^2\Sigma^+ \leftarrow {}^2\Pi_{3/2}$ system, $Q_{12}(N'')$ for $X^2\Pi_{1/2}$, and using eq 9 with unresolved emission, we report in Figure 4 the predicted electric field dependent LIF intensities for the two rotational states of our $|J\Omega M\rangle$-selected beam, the $|{}^3/_2 \pm {}^3/_2 \pm {}^3/_2\rangle$ and $|{}^3/_2 \pm {}^3/_2 \pm {}^1/_2\rangle$ states, along with a few other states of general interest for comparison. The curves for the $|{}^3/_2 \pm {}^3/_2 \pm {}^1/_2\rangle$, $|{}^5/_2 \pm {}^3/_2 \pm {}^3/_2\rangle$, and $|{}^5/_2 \pm {}^3/_2 \pm {}^1/_2\rangle$ rotational states have maximum LIF intensity at $\theta_0 = 0°$ in contrast to the $|{}^3/_2 \pm {}^3/_2 \pm {}^3/_2\rangle$ and $|{}^5/_2 \pm {}^3/_2 \pm {}^5/_2\rangle$ rotational states whose greatest intensity occurs at $\theta_0 = 90°$. The $|{}^1/_2 \pm {}^1/_2 \pm {}^1/_2\rangle$ state has constant intensity with respect to changing polarization excitation. For the two selected states, marked differences are predicted for the polarized LIF intensities. These results are sensible if one considers that the molecular axis is dominantly aligned with the orienting electric field vector (transition dipole perpendicular) for the $|{}^3/_2 \pm {}^3/_2 \pm {}^3/_2\rangle$ state while the molecular axis is on average nearly perpendicular to the orienting field vector (transition dipole aligned with the orienting field) for the $|{}^3/_2 \pm {}^3/_2 \pm {}^1/_2\rangle$ state. Recall (see Table 1) only one alignment moment C_2 is present with opposite signs for the two $|{}^3/_2\ {}^3/_2\ \mathrm{M}\rangle$ states. Less graphical arguments must be made for the LIF polarization dependencies for the $|J = {}^5/_2$, $|\Omega| = {}^3/_2\rangle$ states since higher alignment moments ($C_{n\,=\,4}$) contribute to the orientational probability distributions that govern the LIF signal. The $|{}^1/_2 \pm {}^1/_2 \pm {}^1/_2\rangle$ rotational state does not exhibit a polarization dependence since its distribution does not contain any nonzero alignment moments.

Since the electric field mixes both Λ-doublet parity states with pure parity given at zero field and 50% mixtures in the high-field limit, it is possible to monitor the fluorescence change with orienting electric field strength, i.e., the contribution of a single parity to the rotational state. To follow the evolution of a single parity level (that which corresponds to the pure upper Λ-doublet at zero field) with field strength, one must know the field-dependent coupling between the two states. For the upper Λ-doublet, as mentioned previously, the state is pure f symmetry (−parity) in the low-field limit. The electric field couples the two zero field rotational wave functions, mixing the parity states. As the field strength increases, the f symmetry (−parity) character decreases, and the *e* symmetry (+parity) character increases. The excitation wavelength differs for the two different parities since absorption transitions only connect $+ \leftrightarrow -$ parities. The LIF signal decreases with increasing orienting electric field strength due to less absorption occurring due to a lower amount of f symmetry (−parity) character. Figure 4 illustrates this field dependence of the LIF intensity. Note, in contrast to Figure 3, the field strength axis in Figure 4 increases going into the plane of the figure allowing more detail of the contour to be shown.

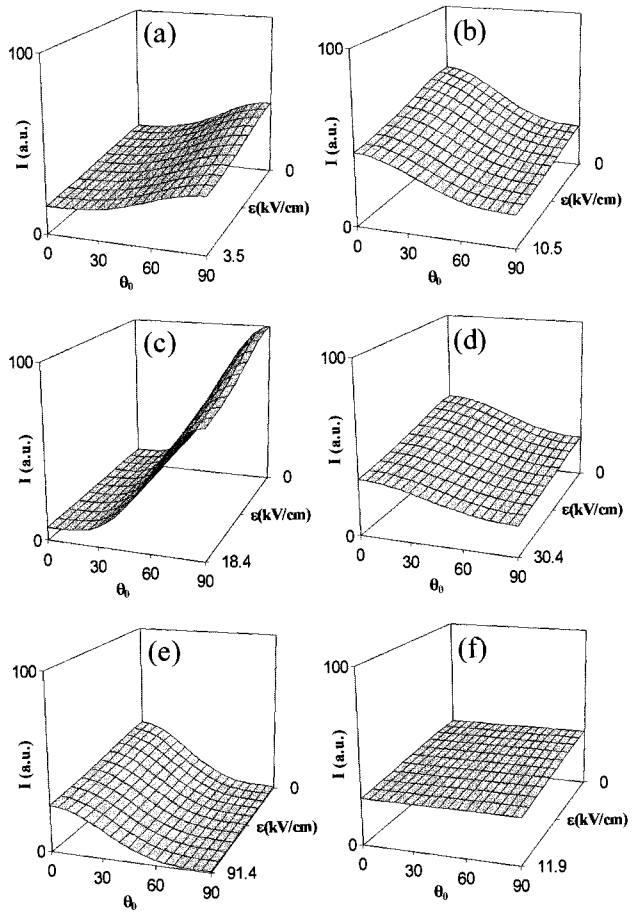

Figure 4. Electric field dependent laser induced fluorescence intensities (*I*) in arbitrary units versus polarization angle with respect to the laboratory-frame orienting electric field vector are plotted for the (a) $|{}^3/_2 \pm {}^3/_2 \pm {}^3/_2\rangle$, (b) $|{}^3/_2 \pm {}^3/_2 \pm {}^1/_2\rangle$, (c) $|{}^5/_2 \pm {}^3/_2 \pm {}^5/_2\rangle$, (d) $|{}^5/_2 \pm {}^3/_2 \pm {}^3/_2\rangle$, (e) $|{}^5/_2 \pm {}^3/_2 \pm {}^1/_2\rangle$, and (f) $|{}^1/_2 \pm {}^1/_2 \pm {}^1/_2\rangle$ rotational states of the hydroxyl radical.

To derive the predicted LIF intensities we calculated the *J* alignment from the moments of the orientational probability distributions; however, the point is to eventually measure absorption-polarized LIF intensities and derive the orientational distribution. The alignment parameters in eq 9 refer to the initial state total angular momentum spatial distribution, however; we are instead interested in the molecular axis distribution. These two systems are connected via the multipole moments of the state, $\langle T(J)^\dagger_{k0}\rangle$, as shown below:[45]

$$\langle T(J)^\dagger_{k0}\rangle = A_0^{(k)}\, b^{(k)}\,(J)\,(2k+1)^{1/2} \qquad (12)$$

where $b^{(k)}(J)$ is a renormalization constant absorbed into $\omega(k_d, k_a, k; J_i'', J', J_f'')$ in eq 9. The orientational probability distribution function given in terms of the multipole moments of the state may be recast as

$$P(\cos\theta, \epsilon) = \left(\frac{2J+1}{4}\right)\sum_{k=0}^{2J}\langle T(J)^{\dagger}_{k0}\rangle Y_{k0}(\theta, \varphi)\left\{[a(\epsilon) + b(\epsilon)]^2(-1)^{M-\Omega}\begin{bmatrix} J & J & k \\ \Omega & -\Omega & 0\end{bmatrix} + [a(\epsilon) - b(\epsilon)]^2(-1)^{M+\Omega}\begin{pmatrix} J & J & k \\ -\Omega & \Omega & 0\end{pmatrix}\right\} \quad (13)$$

with

$$Y_{k0}(\theta, \varphi) = (2k+1)^{1/2}P_k(\cos\theta) \quad (14)$$

It must be noted that using linearly polarized radiation, only $k = 0$ (population) and even k (alignment) moments can be determined experimentally; however, work by Kummel, Sitz, and Zare[46] indicates that experiments with elliptically polarized light can determine all the relevant moments, i.e., odd k moments are also collected. We do not consider this more complicated experiment here. Nonetheless, measuring the even moments and parity state composition using linearly polarized light will provide a valuable consistency check for our calculated orientational distribution functions.

4. Conclusions

This article provides a summary of the quantum mechanical formalism needed to calculate the orientational probability distribution functions (opdfs) for any $^2\Pi$ diatomic molecule as a function of applied field. The calculated opdfs for some hexapole-selectable states of OH vary dramatically with field strength. For the $|^3/_2 \pm {}^3/_2 \pm {}^3/_2\rangle$ states the orientation (C_1) moment of the distribution changes continuously from $C_1 = 0$ in the low-field limit to $C_1 = 0.441$ in the high-field limit. These values demonstrate an ability to systematically adjust the opdf for these states from a highly "aligned" distribution at low field to a highly "oriented" distribution at high fields. This experimental control of orientation should be extremely useful in studies of the stereodynamics of chemical reactivity.

The probability that an OH radical will absorb a linearly polarized photon depends on the relative *alignment* of the transition dipole in the molecular frame and the photon polarization angle in the laboratory frame. Therefore, simple laser induced fluorescence (LIF) measurements using linearly polarized light may be used to measure the total angular momentum alignment and parity state dependence on the applied field and thus deduce the field dependent molecular axis distribution. Section 3 has summarized the quantal formalism needed to calculate LIF yields as a function of laser polarization angle and the strength of an applied "orienting" field. Calculations based on this formalism using opdfs for various hexapole-selectable states of OH show that LIF measurements should indeed provide a good experimental test to validate the opdfs calculated in Section 2.

Acknowledgment. This work was funded by the NSF NYI Program (Grant CHE9457382). We are indebted to Professor Michael D. Morse for many fruitful discussions. We gratefully acknowledge the meticulous efforts of one reviewer whose comments helped improve this article.

References and Notes

(1) *J. Phys. Chem. A* **1997**, *101* (Stereodynamics of Chemical Reactions. Special issue.).
(2) Orr-Ewing, A. J. *J. Chem. Soc., Faraday Trans.* **1996,** *92*, 881.
(3) Loesch, H. J. *Annu. Rev. Phys. Chem.* **1995**, *46*, 555.
(4) Orr-Ewing, A. J.; Zare, R. N. *Annu. Rev. Phys. Chem.* **1994**, *45*, 315.
(5) Levine, R. D. *J. Phys. Chem.* **1990**, *94*, 8872.
(6) *J. Chem. Soc., Faraday Trans. 2*, **1989**, *85* (Orientation and Polarization Effects in Reactive Collisions. Special issue.).
(7) Parker, D. H.; Bernstein, R. B. *Annu. Rev. Phys. Chem.* **1989**, *40*, 561.
(8) *J. Phys. Chem.* **1987**, *91*, 1 (Dynamical Stereochemistry. Special issue.).
(9) Miller, W. H. *Annu. Rev. Phys. Chem.* **1990**, *41*, 245.
(10) Nakamura, H. *Annu. Rev. Phys. Chem.* **1997**, *48*, 299.
(11) Wyatt, R. E., Zhang, J. Z. H., Eds. *Dynamics of Molecules and Chemical Reactions*; Dekker: New York, 1996.
(12) Kliger, D. S.; Lewis, J. W.; Randall, C. E. *Polarized Light in Optics and Spectroscopy*; Academic Press: New York, 1990; Chapter 7.
(13) Meyer, H.; Leone, S. *J. Chem. Phys.* **1996**, *105*, 5858.
(14) Friedrich, B.; Pullman, D. P.; Herschbach, D. R. *J. Phys. Chem.* **1991**, *95*, 8118.
(15) Loesch, H. J.; Remscheid, A. *J. Chem. Phys.* **1990**, *93*, 4779.
(16) Brouard, M.; Simons, J. P. In *Chemical Dynamics and Kinetics of Small Radicals*; Liu, K., Wagner, A., Eds.; World Scientific: London, 1995; Part II, Chapter 18.
(17) Orr-Ewing, A. J.; Zare, R. N. In *Chemical Dynamics and Kinetics of Small Radicals*; Liu, K., Wagner, A., Eds.; World Scientific: London, 1995; Part II, Chapter 20.
(18) Hain, T. D.; Weibel, M. A.; Backstrand, K. M.; Pope, P. E.; Curtiss, T. J. *Chem. Phys. Lett.* **1996**, *262*, 723.
(19) Hain, T. D.; Weibel, M. A.; Backstrand, K. M.; Curtiss, T. J. *J. Phys. Chem. A* **1997**, *101*, 7674.
(20) Schreel, K.; ter Meulen, J. J. *J. Chem. Phys.* **1996**, *105*, 4522.
(21) Schreel, K.; Schleipen, J.; Eppink A.; ter Meulen, J. J. *J. Chem. Phys.* **1993**, *99*, 8713.
(22) Reuss, J. In *Atomic and Molecular Beam Methods*; Scoles, G., Ed.; Oxford University: New York, 1988; Vol. I, Chapter 11.
(23) Stolte, S. In *Atomic and Molecular Beam Methods*; Scoles, G., Ed.; Oxford University: New York, 1988; Vol. I, Chapter 25.
(24) Kuwata, K.; Kasai, T. In *Chemical Dynamics and Kinetics of Small Radicals*; Liu, K., Wagner, A., Eds.; World Scientific: London, 1995; Part II, Chapter 19.
(25) Schreel, K.; ter Meulen, J. J. *J. Phys. Chem. A* **1997**, *101*, 7639.
(26) Alagia, M.; Balucani, N.; Casavecchia, P.; Stranges, D.; Volpi, G. G.; Clary, D. C.; Kliesch, A.; Werner, H.-J. *Chem. Phys.* **1996**, *207*, 389.
(27) Nyman, G.; Clary, D. C. *J. Chem. Phys.* **1994**, *101*, 5756.
(28) Nyman, G. *J. Chem. Phys.* **1996**, *104*, 6154.
(29) Clary, D. C.; Nyman, G.; Hernandez, R. *J. Chem. Phys.* **1994**, *101*, 3704.
(30) Tenner, M. G.; Kuipers, E. W.; Langhout, W. Y.; Kleyn, A. W.; Nicolasen, G.; Stolte, S. *Surf. Sci.* **1990**, *236*, 151.
(31) Curtiss, T. J.; Mackay, R. S.; Bernstein, R. B. *J. Chem. Phys.* **1990**, *93*, 7387.
(32) Pogrebnya, S. K.; Echave, J.; Clary, D. C. *J. Chem. Phys.* **1997**, *107*, 8975.
(33) Zare, R. N. *Angular Momentum;* John Wiley and Sons: New York, 1988; Application 15.
(34) Choi, S. E.; Bernstein, R. B. *J. Chem. Phys.* **1986**, *85*, 150.
(35) Note that we have adopted an alternative sign convention for designating focusable $|J\ \Omega\ M\rangle$ rotational states to that used in our previous publication (ref 19) in order to conform to prevailing standards (see ref 30). For example, previously we labeled the first experimentally focused states as the $|^3/_2 \pm {}^3/_2 \mp {}^3/_2\rangle$ states, and here we label the same states as the $|^3/_2 \pm {}^3/_2 \pm {}^3/_2\rangle$ states.
(36) Brown, J. M.; Kaise, M.; Kerr, C. M. L.; Milton, D. J. *Mol. Phys.* **1978**, *36*, 533.
(37) Corey, G. C.; Alexander, M. H. *J. Chem. Phys.* **1988**, *88*, 6931.
(38) Anderson, R. W. *J. Phys. Chem. A* **1997**, *101*, 7664.
(39) Bulthuis, J.; van Leuken, J.; van Amerom, F.; Stolte, S. *Chem. Phys. Lett.* **1994**, *222*, 378.
(40) This effect is easily included in the Hamiltonian for OH by considering interactions between the ground $X^2\Pi_\Omega$ and first excited electronic state $A^2\Sigma^+$.
(41) Townes, C. H.; Schawlow, A. L. *Microwave Spectroscopy*; Dover: New York, 1975; page 253.
(42) Silver, J. A.; Dimpfl, W. L.; Brophy, J. H.; Kinsey, J. L. *J. Chem. Phys.* **1976**, *65*, 1811.
(43) Greene, C. H.; Zare, R. N. *J. Chem. Phys.* **1983**, *78*, 6741.
(44) Vasudev, R.; Zare, R. N.; Dixon, R. N. *J. Chem. Phys.* **1984**, *80*, 4863.
(45) Blum, K. *Density Matrix Theory and Applications*, 2nd ed.; Plenum Press: New York, 1996; Chapter 7.
(46) Kummel, A. C.; Sitz, G. O.; Zare, R. N. *J. Chem. Phys.* **1988**, *88*, 7357.